Reduction of moisture sensitivity of PbS quantum dot solar cells by incorporation of reduced graphene oxide

Beatriz Martín-García,[a] Yu Bi,[b] Mirko Prato,[a] Davide Spirito,[a] Roman Krahne,[a] Gerasimos Konstantatos[b,c] and Iwan Moreels[a,†,]*

[a]Istituto Italiano di Tecnologia, Via Morego, 30, 16163 Genova, Italy.

[b]ICFO-Institut de Ciencies Fotoniques. The Barcelona Institute of Science and Technology, Av. Carl Friedrich Gauss 3, 08860 Castelldefels (Barcelona), Spain.

[c]ICREA-Intitucio Catalana de Recerca I Estudis Avancats, Lluis Companys 23, 08010 Barcelona, Spain.

Present Address:

†Iwan Moreels. Department of Chemistry, Ghent University. Krijgslaan 281-S3, 9000 Gent, Belgium.

Corresponding author:

*Iwan Moreels. E-mail: iwan.moreels@ugent.be

Sol. Energy Mater. Sol. Cells, 183, 1-7 (2018), doi.org/10.1016/j.solmat.2018.04.005

ABSTRACT. PbS nanocrystals are an important narrow-gap material for solar cells and photodetectors. Nevertheless, their application may be limited because device performance can be affected by atmospheric conditions. Indeed, the presence of oxygen and/or water can degrade the active layers, possibly leading to device failure. Strategies to address this issue are therefore actively explored. Here we report a solution-processed PbS quantum dot solar cell, consisting of a PbS-silane functionalized reduced graphene oxide (PbS-rGO) layer on top of the PbS absorber film, which enhances device stability, especially when the solar cells are exposed to moisture. Power conversion efficiency (PCE) measurements demonstrate a slower degradation under continuous illumination for solar cells with PbS-rGO. When storing the samples under saturated water vapor, differences are even more remarkable: with PbS-rGO the solar cells essentially maintain their initial PCE, while the PCE of the PbS reference devices is reduced by 50% after 5 days. Scanning electron microscopy, energy dispersive X-ray and X-ray photoelectron spectroscopy reveal the damage to the PbS films and the formation of $PbSO_x$ crystals in the PbS reference devices. Such crystals are not observed in the PbS-rGO devices, further supporting the importance of the PbS-rGO barrier layer.

KEYWORDS: nanocrystals, reduced graphene oxide, photovoltaics, stability, moisture.

1. Introduction

Lead sulfide quantum dots (QDs) have demonstrated to be highly suitable materials for solution-processed solar cells, currently reaching power conversion efficiencies (PCE) up to 11.6%.[1] Fast, sensitive and broad-band near-infrared photodetectors based on PbS QDs have also been implemented in a variety of architectures.[2] However, the degradation of such devices under ambient conditions remains an important challenge for practical applications. In presence of oxygen, byproducts such as PbO, $PbSO_3$ or $PbSO_4$ can form and reduce the device performance.[3,4] Focusing on solar cells, several strategies have been proposed to address this issue, involving QD surface passivation with ligands,[5,6] optimization of the device layer architecture,[7,8] or device encapsulation.[9] Studies were mostly designed to improve the shelf life[7,10], or the stability under continuous illumination.[3,6,11] However, another important parameter, the relative humidity (R.H.) in ambient atmosphere, has not received similar attention so far. In several areas (excluding deserts or high altitudes), the long-term average R.H. can exceed 70%,[12] hence values clearly surpass typical laboratory conditions of 30-50%. Humidity has already shown to degrade solar cells based on perovskites,[13,14] or organic materials[15,16], and therefore stability under humid conditions is an important issue that needs to be addressed.

Here, we increased the stability of PbS QD solar cells under both dry and humid atmosphere by adding a spin-coated top layer consisting of a PbS-reduced graphene oxide (PbS-rGO) hybrid material[17]. Previously, inclusion of graphene or graphene oxide has been shown to yield PbS solar cells with good power conversion efficiency (PCE),[18,19] although device stability was not investigated. However, organic (OPV) and perovskite-based photovoltaics have already experienced the advantages of rGO integration, with prolonged stability under ambient conditions. In OPV, even if the initial performance was not improved by rGO inclusion,[20,21] the lifetime

of the device can be increased by 50% under 100% R.H. conditions[21]. In the case of perovskites,[22–24] studies were carried out in air with only ≤ 50% R.H. Already under these conditions, the endurance tests showed an efficient suppression of the material degradation. More specifically, when using spiro-rGO[22] the solar cells almost retained the initial PCE after 120h, while with PCBM-rGO[24] the PCE is reduced from 13.5 to 7% (52% retention) after 120h. This in contrast with the reference cells, that passed from a PCE of 12% to 1% already after 50h.

In this work we show that rGO inclusion in PbS QD solar cells yields a significant improvement in stability compared to corresponding PbS-only devices,[6] even under R.H. 100% conditions. Our devices retained 96% of the initial PCE after 120 h (5 days) of continuous exposure to a saturated water vapor atmosphere, in stark contrast to the PbS-only reference cells, whose PCE nearly halved after the same treatment. Characterization of the PbS film morphology after exposure showed that the rGO reduces structural damage caused by humidity. Hence, our results hold great promise to stabilize the performance of PbS and other solution-processed solar cells, which can suffer similar degradation processes in presence of moisture.

2. Materials and Methods

2.1. PbS QD and rGO synthesis. PbS QDs[6] and rGO[17] are prepared according to established methods. The PbS are coupled to the rGO sheets using 3-mercaptopropyltrimethoxysilane, as outlined in ref. [17]. Further details are provided in the SM.

2.2. Solar cell fabrication. We prepared the ITO/ZnO/QD_{EMII}/QD_{EDT} solar cells following Cao *et al*.[6] The device was constructed using layer-by-layer spin coating in air (R.H. ≤ 50%). For the ligand exchange on the PbS QD thin films, EMII (7 mg.mL^{-1} in MeOH) and EDT (0.02 vol% in ACN) solutions were used, respectively. The reference cell consisted of 12 PbS_{EMII} layers and 2

PbS_{EDT} layers. In the case of the PbS-rGO solar cell, we replaced the second PbS_{EDT} layer (10 nm thick) with a PbS-rGO_{EDT} layer (44 nm thick, determined by cross section SEM measurements, [SM, **Fig. S1e-f**]). To deposit this layer, the PbS QD-rGO dispersion was spin coated at 700 rpm for 120 s. Then, the film was covered by an EDT solution in ACN for 30 s before spin coating at 2500 rpm for 40 s. The substrate was rinsed three times by placing several drops of ACN, followed by spinning at 2500 rpm for 40 s to dry the film. All solar cells were stored in a N_2-filled glove box overnight before thermal deposition of a 100 nm Au layer (deposition rate of 0.5 $Å.s^{-1}$) in a Kurt J. Lesker Nano 36 system (base pressure < 1.0 10^{-6} mbar). The final devices, with an Au contact area of 0.03 cm^2, were taken out from the evaporator and transferred into the glove box for annealing at 80 ^oC for 5 min.

2.3. Photovoltaic characterization of the devices. *J-V* curves were recorded in air using a Keithley 2400 source meter under 100 $mW.cm^{-2}$ (AM1.5G) illumination, provided by a Newport sol3A (class AAA) solar simulator (freshly prepared devices) or a LOT-Oriel LSH601/LSZ163 solar simulator (stability tests). The light intensity was calibrated with a Newport 91150V reference cell in both cases. The external quantum efficiency was measured with a lock-in amplifier (Stanford Research System SR830) under chopped monochromatic light, generated by a xenon lamp passing through a Newport Cornerstone 260 monochromator. The R.H. in the lab was kept between 40-60%.

2.4. Continuous illumination and water exposure of solar cells. For the stability under AM1.5 illumination conditions, the samples were continuously exposed in air (R.H. 40-60%). For the exposure to a controlled humidity, samples were placed in a closed glass recipient (250 cm^3) at saturated water vapor atmosphere (R.H. 100%) under ambient light at 25°C, and removed only for the *J-V* characterization. The R.H. 100% was generated by adding MilliQ® water to the container and placing it on a hot plate (50 °C), ensuring that condensation occurs on the sidewalls

of the container and not on the samples. During the exposure, no liquid drops were observed on the films. In all tests, we carried out measurements on at least 2 samples for each type of device. Furthermore, the reported trends result from the measurement of the three best solar cells in each sample, which contained eight devices overall.

2.5. UPS-XPS characterization. To estimate the energy of the valence band maximum (VBM) and conduction band minimum (CBM) of the materials, ultraviolet photoelectron spectra were collected with a Kratos Axis UltraDLD spectrometer, using a He I (21.2 eV) discharge lamp, equipped with a charge neutralizer system used on all specimens analyzed. The samples for UPS were prepared by spin coating a thin film of PbS QDs and PbS-rGO, respectively, onto 50 nm-Au sputtered coated silicon wafers. We use the same experimental procedures as for the solar cell fabrication. A −9.0 V bias was applied to the sample in order to precisely determine the low kinetic energy cut-off, following a reported procedure.[25] The work function (WF) was measured from the threshold energy of the secondary electron emission during He I excitation. The position of the VBM vs. vacuum level was estimated by subtracting, from the WF, the energy obtained by linear extrapolation of the low binding energy onset of the UPS.[26] The CBM was calculated by adding the optical band gap (1.3 eV) to the VBM. X-ray photoelectron spectroscopy was carried out using the same equipment as for UPS, using a monochromatic Al Kα source (15 kV, 20 mA) and the charge neutralizer system. High-resolution scans were performed at a constant pass energy of 10 eV and steps of 0.1 eV. The photo-electrons were detected at a take-off angle $\varphi = 0°$ with respect to the surface normal. The pressure in the analysis chamber was kept below 7×10^{-9} Torr. Spectra have been charge corrected to the main line of the carbon 1s spectrum (adventitious carbon) set to 284.8 eV. The spectra were analyzed using the CasaXPS software (version 2.3.16). Samples for XPS consisted of PbS_{EMII} (12 layers) and PbS_{EDT} (2 layers) for the reference film, and PbS_{EMII} (12 layers), PbS_{EDT} (1 layer) and PbS-rGO_{EDT} (1 layer) for the PbS-rGO film. Both were deposited on

plasma-cleaned glass substrates (100W, 60s, 100% N_2), and were prepared in a glovebox to avoid oxidation. After the first XPS measurement series, the samples were exposed to a water saturated vapor atmosphere for 5 days, after which the XPS measurements were repeated.

2.6. SEM/EDX characterization. We performed SEM/EDX measurements on the solar cells and complementary samples using a Helios Nanolab 600 (FEI Company) microscope combined with an X-Max detector and INCA® system (Oxford Instruments) for the EDX spectra acquisition and analysis. SEM measurements were performed at 10-20 kV and 0.2 nA, while EDX measurement conditions were set at 10kV and 0.8nA.

3. Results and Discussion

The solar cell architecture is based on a PbS depleted heterojunction, using 1-ethyl-3-methylimidazolium iodide (EMII) and 1,2-ethanedithiol (EDT) ligands for the bottom and top PbS QD layer, respectively, which has already yielded PbS QD solar cells with a certified PCE of 8.7%.[6] Before incorporation into the solar cells, the rGO flakes were functionalized with (3-mercaptopropyl)trimethoxysilane ligands and subsequently coupled with PbS QDs [Supplementary Material (SM), **Fig. S1a**], as described in Ref. [17]. The resulting hybrid material formed a close-packed thin film after spin coating from an ethanol dispersion [SM, **Fig. S1b-e**]. Similar to PbS QD films,[27] the conductance of the PbS-rGO thin films increased by more than one order of magnitude when replacing the oleic acid ligands with EDT using a solid ligand exchange procedure[7] [SM, **Fig. S2**]. To ensure that the EDT-treated PbS-rGO films possess the correct band alignment for the solar cells, we characterized them by UV photoelectron spectroscopy (UPS) [SM, **Fig. S3**]. From the UP spectrum, a work function of -4.1 eV and a valence band maximum at -5.1 eV vs. vacuum level were calculated, yielding a band offset of 300

meV with the PbS_{EMII} layer, which demonstrates that the EDT-exchanged PbS-rGO film is suitable as hole transporting layer in the final device (**Fig. 1a**).

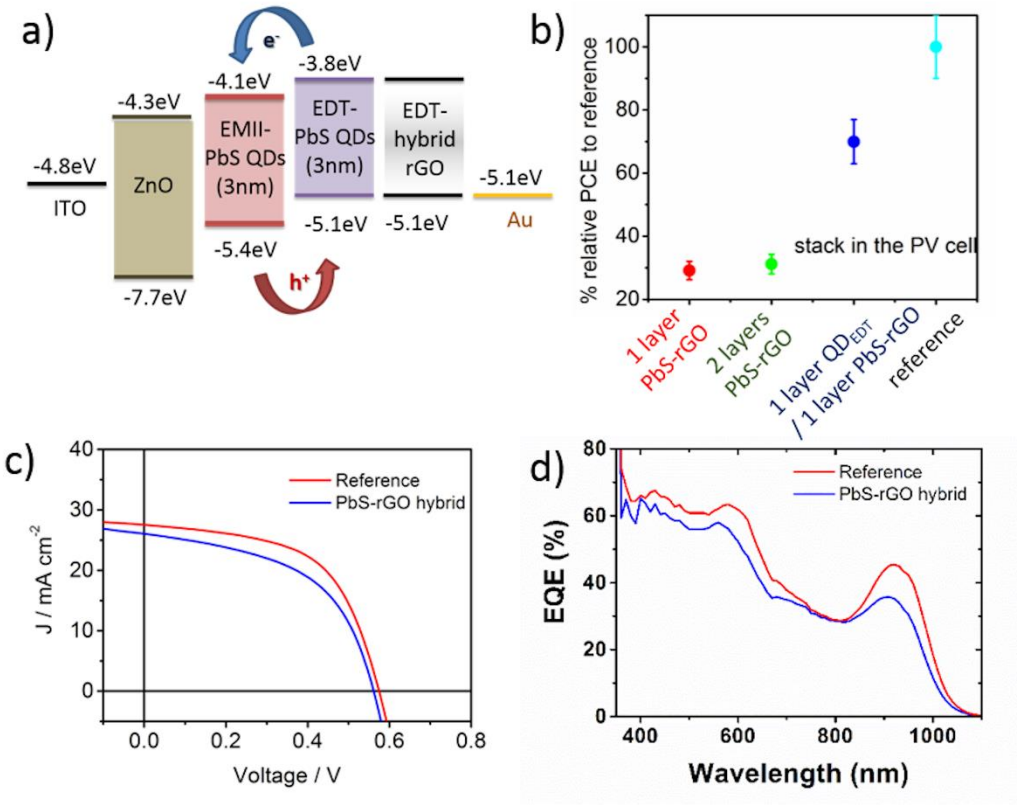

Figure 1. (a) Band alignment determined from UPS for the materials comprising the PbS/PbS-rGO solar cells. ITO, ZnO and Au values are taken from Brown et al.[28,29] (b) Relative PCE for the different layouts on top of EMII-exchanged PbS QD layers [see SM, Table S1]. The reference (cyan) has a 20 nm PbS_{EDT} layer, while the other samples combine either: 1 layer (44 nm) of PbS-rGO (red), 2 layers of PbS-rGO (100nm, green) and 1 layer PbS_{EDT} (10 nm) + 1 layer PbS-rGO (44 nm, blue). (c) J-V curves obtained for the best reference (PCE 9.0%, J_{sc} 27.51 mA cm^{-2}, V_{oc} 0.57 V and FF 0.57) and PbS-rGO (PCE 7.6%, J_{sc} 26.02 mA cm^{-2}, V_{oc} 0.56 V and FF 0.52) devices after 30 days ageing. (d) The corresponding EQE curves for the same devices as-prepared: reference (PCE 7.7%, J_{sc} 21.42 mA cm^{-2}, V_{oc} 0.56 V and FF 0.64) and PbS-rGO (PCE 6.7%, J_{sc} 21.17 mA cm^{-2}, V_{oc} 0.56 V and FF 0.56).

In the fabricated solar cells we inserted the EDT-treated PbS-rGO film as top layer (i.e. directly underneath the Au top electrode). *J-V* measurements on the different solar cells yielded the PCE. After PCE optimization by varying the thickness and position of the PbS-rGO absorber layer (**Fig. 1b** and SM, **Table S1**), we obtained the following optimized design: keeping the same PbS_{EMII} layer, the original 20 nm PbS_{EDT} layer[6] can be replaced by a 10 nm PbS_{EDT} layer, with a

44 nm PbS-rGO$_{EDT}$ layer on top [SM, **Fig. S1c-d**]. Possibly, the 10 nm layer of PbS$_{EDT}$ (*i.e.* without rGO) remains necessary in order to prevent direct contact between the PbS$_{EMII}$ layer and the Au top electrode via metallic rGO flakes.

When storing the samples under dark conditions in air, they revealed an enhancement of the PCE [SM, **Fig. S4**].[6] After 30 days, samples reached average (best) PCE values of 8.2% (9.0%) and 5.7% (7.6%) for the PbS reference and PbS-rGO devices, respectively. The somewhat lower PCE for PbS-rGO solar cells stems mainly from a reduction of the short-circuit current density (J_{sc}) (**Fig. 1c**) induced by the rGO flakes. Note that a lower J_{sc} was also observed in perovskite solar cells that incorporated rGO (40% PCE reduction).[23] In **Fig. 1d** we compare the external quantum efficiency (EQE) of the PbS reference cell with the optimized PbS-rGO device. The presence of rGO does not modify the overall shape of the curve, yet it slightly reduces the EQE. Therefore, the J_{sc} values obtained from integrating the EQE spectra in as-prepared samples are lower for the PbS-rGO sample (15.7 mA cm^{-2}) than for the reference (17.7 mA cm^{-2}). Possibly, the decrease in the EQE, which also translates into lower PCE values, is due to absorption in the metallic rGO. Moreover, the $J_{sc\text{-}EQE}$ values are lower than the results obtained the same day from the J-V measurements that yielded 21.4 (reference, PCE 7.7%) and 21.2 mA cm^{-2} (PbS-rGO, PCE 6.7%). This mismatch between $J_{sc\text{-}EQE}$ and J_{sc} can be ascribed to a UV exposure photo-doping effect during the J-V measurements under the solar simulator lamp, as we already observed on EMII-treated PbS QD solar cells.[30]

As already mentioned, a requirement for practical applications of solar cells is good stability under prolonged light exposure and conditions of varying humidity. **Fig. 2** reports the results for a continuous (AM1.5) illumination of the solar cells under ambient atmosphere [see also SM, **Fig. S5** for the evolution of J_{sc}, V_{oc} and FF]. When analyzing the average behavior of the different solar cells (dash-dotted lines), the average PCE in the reference cells decreases from 7.2% to 6.2% after

35 h (relative reduction of 14%), in line with previous results.[6] Exposure up to 168 h finally yielded a PCE of 3.9% (46% reduction). Although the solar cells with a PbS-rGO layer displayed a lower initial PCE, after 168 h we observed a smaller reduction of only 37%. While the slower degradation yields promise for long-term stability, it is nevertheless not sufficient for the PbS-rGO devices to surpass the PCE of the PbS reference devices over the duration of the current experiments.

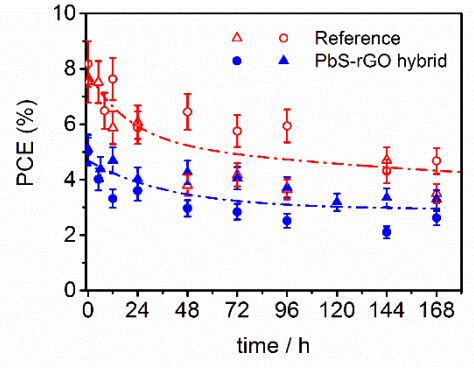

Figure 2. PCE evolution for different solar cells under continuous illumination (AM1.5) and ambient conditions. We prepared in total two substrates with PbS reference devices (red) and two with PbS-rGO (blue). On each substrate, we measured 3 devices. The dashed lines are exponential fits $[y\,(PCE\%) = C + A_0 e^{-x(t)/\tau}]$ that yield the average behavior of both types of solar cells: reference (τ = 38.2 h, y(t=0) = 8%, C= 4.2%, A_0=3.8%) and PbS-rGO (τ = 40.8 h, y(t=0) = 4.8%, C= 3%, A_0=1.8%,), respectively.

In contrast, when exposing the samples to a water saturated vapor atmosphere (R.H. 100%) at room temperature, results are markedly different, as shown in **Fig. 3a** [see also SM, **Fig. S6** for the evolution of J_{sc}, V_{oc} and *FF*]. Without the PbS-rGO layer, we observed a significant decrease of the average PCE from 7.1% to 3.7% after 120 h of exposure, while in the case of the PbS-rGO solar cells, the average PCE is almost fully retained over the entire duration of the experiment. Here, due to the strong degradation of the reference cells, absolute values of the PbS-rGO devices surpass the reference already after less than 24 h of exposure. The evolution of the full *J-V* curves for the moisture test is shown in **Fig. 3b-c**, where a systematic loss in J_{sc} and *FF* can be observed

for the reference sample, leading to the decrease of PCE. In contrast, for the PbS-rGO sample, we obtained an almost constant J_{sc}, allowing us to retain the PCE.

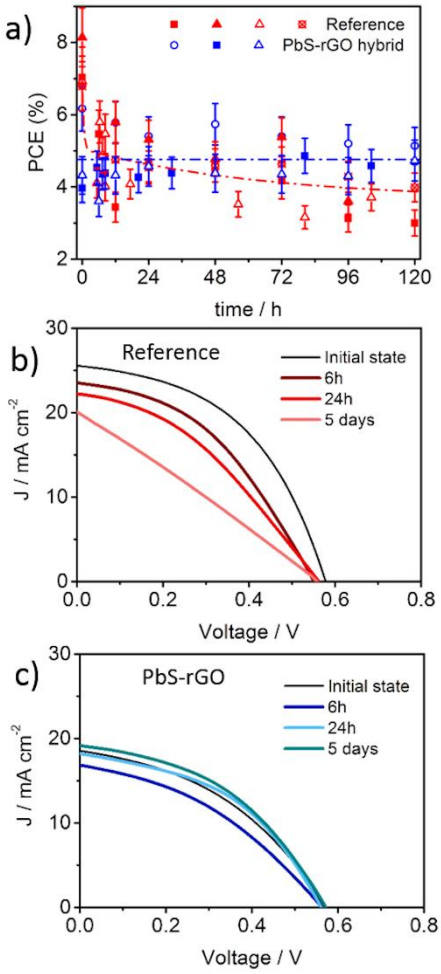

Figure 3. Evolution of the PCE (a) and *J-V* curves (b, c) for different solar cells under exposure to saturated water vapor atmosphere. We prepared in total four substrates with PbS reference devices (red) and three with PbS-rGO (blue). On each substrate, we measured 3 devices. The dashed lines are exponential fits that yield the average behavior of both types of solar cells.

The degradation of the reference solar cells can be appreciated not only as a loss in PCE, but also in a progressive change in their surface color from dark brown to white (**Fig. 4a-b**) [see also SM, **Fig. S7** for samples before exposure]; this color change is not observed on the PbS-rGO samples. To gain further insight into the species formed at the solar cell surface during the moisture

exposure, we carried out XPS analysis on thin films prepared similarly to the PbS and PbS-rGO solar cells. Specifically, we spin-coated the PbS_{EMII} and PbS_{EDT}, or $PbS\text{-}rGO_{EDT}$, layers directly on glass. Since the last layer corresponds to EDT-treated PbS QDs, we focused the analysis on the sulfur components. Evaluating the evolution of the S 2p XPS spectrum before (**Fig. 4c**) and after (**Fig. 4d**) moisture exposure, in the PbS reference sample we detected the formation of polysulfides, SO_3^{2-} and SO_4^{2-}, while the relative signal of S^{2-} (ascribed to PbS) and free thiol species (due to the EDT functionalization) decreases. Results are in line with a partial hydrolyzation and oxidation of the PbS_{EDT} surface, as already discussed by Nozik *et al*.[31] in air-exposed PbSe QD films, and by Sargent *et al*.[3] in ageing tests on PbS QD films. Notably, for the PbS-rGO samples (**Fig. 4e-f**), SO_x^{2-} species are also observed (orange and dark green S 2p doublet peaks from 165 eV to 168 eV). Moreover, the formation of polysulfides –likely oxidation products from the EDT and S^{2-} moieties of the silane– is largely increased (red S 2p doublet peak at 163.2 eV / 164.4 eV) with respect to the reference sample. Pb 4f XPS spectra confirm the formation of $PbSO_x$ (**Fig. 4 g-j**). After moisture exposure of reference and PbS-rGO samples, two additional peaks can be distinguished, related to $PbSO_3$ (138.6 eV Pb $4f^{7/2}$) and $PbSO_4$ (139.6 eV Pb $4f^{7/2}$) species[32].

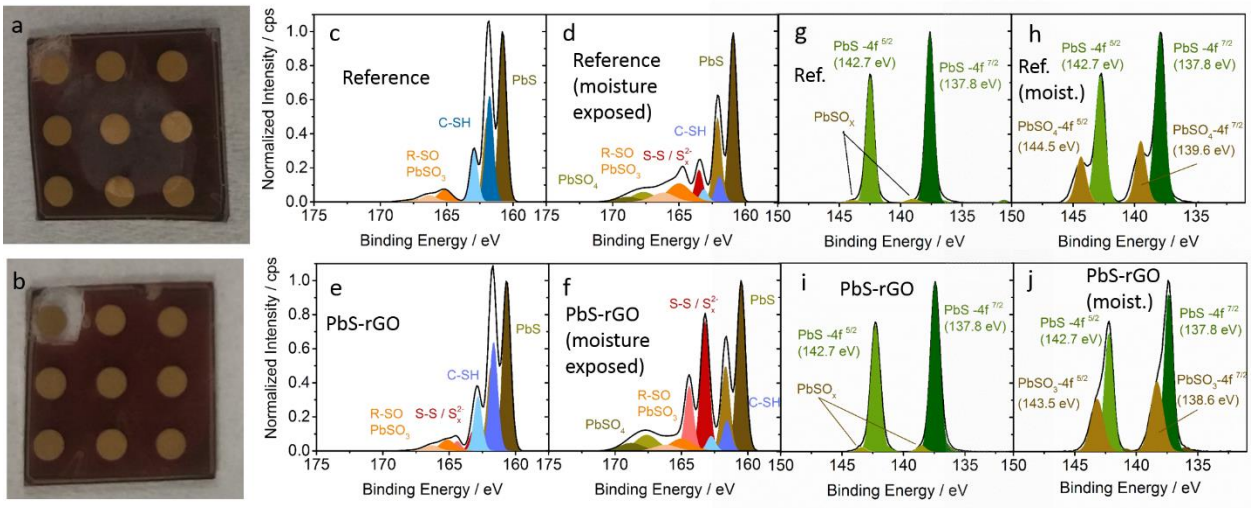

Figure 4. (a-b) Representative pictures of PbS reference cells (a) and PbS-rGO cells (b) after exposure to a 100% R.H. atmosphere for 5 days. In the center of the substrate, a white patch can be observed in the reference cells, which does not appear in the PbS-rGO sample. (c-f) XPS S 2p core level spectra of the PbS reference (c, d) and PbS-rGO (e, f) thin films before and after moisture exposure. (g-j) XPS Pb 4f core level spectra of the PbS reference (g, h) and PbS-rGO (i, j) thin films before and after moisture exposure. The films correspond to PbS_{EMII} (12 layers) / PbS_{EDT} (2 layers) for the reference and PbS_{EMII} (12 layers) / PbS_{EDT} (1 layer) / PbS-rGO_{EDT} (1 layer) for the PbS-rGO.

We also carried out scanning electron microscopy (SEM) combined with energy dispersive X-ray spectroscopy (EDX). SEM-EDX results on reference cells before [SM, **Fig. S8a-b**] and after (**Fig. 5a-c**) moisture exposure revealed that the white area corresponds to oxidized regions, leading to the growth of hexagonal microcrystals (**Fig. 5a**, red square and SM, **Fig. S8c**]. The EDX data (red area, **Fig. 5a-b**), are in line with the results from XPS (**Fig. 4c-d**). More specifically, the detection of the elements Pb, S and O in the microcrystals formed after moisture exposure is consistent with the increase of SO_x^{2-} compounds observed with XPS (**Fig. 4c-d**). We can thus conclude that we form $PbSO_x$ hexagonal microcrystals.

We observed that the formation of these crystals is accompanied by voids in the PbS QD film (**Fig. 5a**, green square). The resulting thinner top layer leads to increased signatures of the underlying PbS_{EMII} film, ZnO electron-transport layer and even the ITO-glass substrate, as evidenced by an increased amount of iodine, zinc, indium and tin detected in degraded samples (**Fig. 5c**). In contrast, for the PbS-rGO samples, SEM images and associated EDX spectra before (**Fig. 5d-f**) and after exposure (**Fig. 5e-f**) do not display significant differences, confirming the increased device stability in humid conditions by integration of a PbS-rGO top layer underneath the Au contact. As we observed the $PbSO_x$ formation only in XPS (**Fig. 4e-f**), while the film morphology remains unaffected as evidenced by SEM and EDX [**Fig. 5e-f** and SM, **Fig. S8e**], XPS data suggest that oxidation is not completely avoided in humid conditions, however, it is restricted to the film surface for PbS-rGO solar cells, while in the PbS reference cells it results in material recrystallization throughout the entire film.

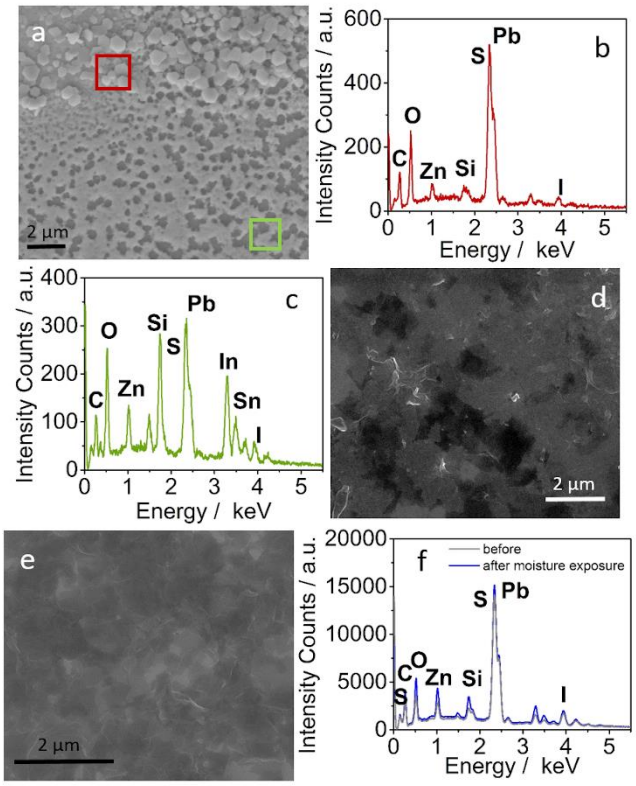

Figure 5. (a) Representative SEM image of a PbS reference cell (area outside Au contact) after moisture exposure. The film shows the formation of $PbSO_x$ crystals (red square, ca. 2.5 μm^2) and voids in the film (green square, ca. 2.5 μm^2). (b-c) The corresponding EDX spectra from the red and green marked regions confirm the $PbSO_x$ formation [increased oxygen peak, see also SM, Figure S9b], and fractures (increased I, Zn, and In/Sn signals from PbS_{EMII}, ZnO and ITO layers), respectively. (d) SEM image of a PbS-rGO solar cell before exposure (area outside Au contact). (e) The SEM image of the PbS-rGO solar cell after moisture exposure shows a similar morphology. (f) Also the EDX spectrum (collected on an area of 160x160 μm^2) remains unaffected.

This conclusion is further supported by absorption spectra measured on PbS and PbS-rGO thin films before and after 5-days exposure to R.H. 100% [SM, **Fig. S9**]. We observed a blue shift of the first absorption peak for PbS QDs, which is absent in the PbS-rGO sample. Thus, the introduction of rGO flakes mitigates the water-induced oxidation, yielding increased device stability in humid conditions. This barrier effect is consistent with previous results where rGO was demonstrated to be highly impermeable to moisture and other gases,[33] and was applied as protective layer in organic[20,21,34] and perovskite[22–24] solar cells. Possibly, the silane

moieties in the PbS-rGO film may also undergo a chemical polymerization reaction with water molecules,[35,36] which may further reduce the degradation of the PbS layer.

4. Conclusions

We have integrated functionalized rGO flakes into PbS QD solar cells, obtaining a PCE up to 7.6% after optimization of the absorber layer layout, which compares well with the PCE of PbS-only reference solar cells. The PbS-rGO film significantly improved the long-term stability under ambient atmosphere, most importantly reducing the degradation of the devices in humid conditions. No significant decay of the PCE was observed for the PbS-rGO solar cells, while the reference devices showed a reduction of about 50% of its initial value after 120 h of exposure. Considering the versatility of the silane-functionalized rGO material, we expect that this strategy can be extended to other QD solar cells, as well as organic and perovskite solar cells, which at present are confronted with similar issues.[34,37,38] The proposed approach can be an effective addition to encapsulation strategies, not only in solar cells but also in other optoelectronic devices such as photodetectors[39,40] and light emitting diodes,[41] to enhance the long-term stability and open a pathway to viable applications in ambient conditions.

5. Acknowledgments

This project has received funding from the European Union's Horizon 2020 research and innovation programme under grant agreement No 696656 (GrapheneCore1). The authors thank to Dr. F. De Angelis for the access to the IIT clean room facilities and M. Leoncini for support during the SEM/FIB measurements and evaporation procedures.

6. References

[1] J. Choi, Y. Kim, J.W. Jo, J. Kim, B. Sun, G. Walters, F.P. García de Arquer, R. Quintero-Bermudez, Y. Li, C.S. Tan, L.N. Quan, A.P.T. Kam, S. Hoogland, Z. Lu, O. Voznyy, E.H. Sargent, Chloride Passivation of ZnO Electrodes Improves Charge Extraction in Colloidal Quantum Dot Photovoltaics, Adv. Mater. 29 (2017) 1702350. doi:10.1002/adma.201702350.
[2] R. Saran, R.J. Curry, Lead sulphide nanocrystal photodetector technologies, Nat Photon. 10 (2016) 81–92. doi:10.1038/nphoton.2015.280.
[3] J. Tang, L. Brzozowski, D.A.R. Barkhouse, X. Wang, R. Debnath, R. Wolowiec, E. Palmiano, L. Levina, A.G. Pattantyus-Abraham, D. Jamakosmanovic, E.H. Sargent, Quantum Dot Photovoltaics in the Extreme Quantum Confinement Regime: The Surface-Chemical Origins of Exceptional Air- and Light-Stability, ACS Nano. 4 (2010) 869–878. doi:10.1021/nn901564q.
[4] G. Zhai, A. Bezryadina, A.J. Breeze, D. Zhang, G.B. Alers, S.A. Carter, Air stability of TiO2/PbS colloidal nanoparticle solar cells and its impact on power efficiency, Appl. Phys. Lett. 99 (2011) 63512. doi:10.1063/1.3617469.
[5] Z. Ning, O. Voznyy, J. Pan, S. Hoogland, V. Adinolfi, J. Xu, M. Li, A.R. Kirmani, J.-P. Sun, J. Minor, K.W. Kemp, H. Dong, L. Rollny, A. Labelle, G. Carey, B. Sutherland, I. Hill, A. Amassian, H. Liu, J. Tang, O.M. Bakr, E.H. Sargent, Air-stable n-type colloidal quantum dot solids, Nat Mater. 13 (2014) 822–828. doi:10.1038/nmat4007.
[6] Y. Cao, A. Stavrinadis, T. Lasanta, D. So, G. Konstantatos, The role of surface passivation for efficient and photostable PbS quantum dot solar cells, Nat. Energy. 1 (2016) 16035. doi:10.1038/nenergy.2016.35.
[7] C.-H.M. Chuang, P.R. Brown, V. Bulović, M.G. Bawendi, Improved performance and stability in quantum dot solar cells through band alignment engineering, Nat. Mater. 13 (2014) 796–801. doi:10.1038/nmat3984.
[8] X.-D. Mai, H.J. An, J.H. Song, J. Jang, S. Kim, S. Jeong, Inverted Schottky quantum dot solar cells with enhanced carrier extraction and air-stability, J. Mater. Chem. A. 2 (2014) 20799–20805. doi:10.1039/C4TA04305G.
[9] A.H. Ip, A.J. Labelle, E.H. Sargent, Efficient, air-stable colloidal quantum dot solar cells encapsulated using atomic layer deposition of a nanolaminate barrier, Appl. Phys. Lett. 103 (2013) 263905. doi:10.1063/1.4858135.
[10] M. Liu, O. Voznyy, R. Sabatini, F.P. Garcia de Arquer, R. Munir, A.H. Balawi, X. Lan, F. Fan, G. Walters, A.R. Kirmani, S. Hoogland, F. Laquai, A. Amassian, E.H. Sargent, Hybrid organic-inorganic inks flatten the energy landscape in colloidal quantum dot solids, Nat Mater. 16 (2017) 258–263. doi:10.1038/nmat4800.
[11] J.M. Luther, J. Gao, M.T. Lloyd, O.E. Semonin, M.C. Beard, A.J. Nozik, Stability Assessment on a 3% Bilayer PbS/ZnO Quantum Dot Heterojunction Solar Cell, Adv. Mater. 22 (2010) 3704–3707. doi:10.1002/adma.201001148.
[12] A. Dai, Recent Climatology, Variability, and Trends in Global Surface Humidity, J. Clim. 19 (2006) 3589–3606. doi:10.1175/JCLI3816.1.
[13] Y. Bai, Q. Dong, Y. Shao, Y. Deng, Q. Wang, L. Shen, D. Wang, W. Wei, J. Huang, Enhancing stability and efficiency of perovskite solar cells with crosslinkable silane-functionalized and doped fullerene, Nat. Commun. 7 (2016) 12806. doi:10.1038/ncomms12806.
[14] L. Hu, G. Shao, T. Jiang, D. Li, X. Lv, H. Wang, X. Liu, H. Song, J. Tang, H. Liu, Investigation of the Interaction between Perovskite Films with Moisture via in Situ Electrical Resistance Measurement, ACS Appl. Mater. Interfaces. 7 (2015) 25113–25120. doi:10.1021/acsami.5b06268.

[15] G. Kakavelakis, D. Konios, E. Stratakis, E. Kymakis, Enhancement of the Efficiency and Stability of Organic Photovoltaic Devices via the Addition of a Lithium-Neutralized Graphene Oxide Electron-Transporting Layer, Chem. Mater. 26 (2014) 5988–5993. doi:10.1021/cm502826f.
[16] T.S. Glen, N.W. Scarratt, H. Yi, A. Iraqi, T. Wang, J. Kingsley, A.R. Buckley, D.G. Lidzey, A.M. Donald, Dependence on material choice of degradation of organic solar cells following exposure to humid air, J. Polym. Sci. Part B Polym. Phys. 54 (2016) 216–224. doi:10.1002/polb.23905.
[17] B. Martin-Garcia, A. Polovitsyn, M. Prato, I. Moreels, Efficient charge transfer in solution-processed PbS quantum dot-reduced graphene oxide hybrid materials, J. Mater. Chem. C. 3 (2015) 7088–7095. doi:10.1039/C5TC01137J.
[18] B.-S. Kim, D.C.J. Neo, B. Hou, J.B. Park, Y. Cho, N. Zhang, J. Hong, S. Pak, S. Lee, J.I. Sohn, H.E. Assender, A.A.R. Watt, S. Cha, J.M. Kim, High Performance PbS Quantum Dot/Graphene Hybrid Solar Cell with Efficient Charge Extraction, ACS Appl. Mater. Interfaces. 8 (2016) 13902–13908. doi:10.1021/acsami.6b02544.
[19] L. Hu, D.-B. Li, L. Gao, H. Tan, C. Chen, K. Li, M. Li, J.-B. Han, H. Song, H. Liu, J. Tang, Graphene Doping Improved Device Performance of ZnMgO/PbS Colloidal Quantum Dot Photovoltaics, Adv. Funct. Mater. 26 (2016) 1899–1907. doi:10.1002/adfm.201505043.
[20] H. Yamaguchi, J. Granstrom, W. Nie, H. Sojoudi, T. Fujita, D. Voiry, M. Chen, G. Gupta, A.D. Mohite, S. Graham, M. Chhowalla, Reduced Graphene Oxide Thin Films as Ultrabarriers for Organic Electronics, Adv. Energy Mater. 4 (2014) 1300986. doi:10.1002/aenm.201300986.
[21] T. Kim, J.H. Kang, S.J. Yang, S.J. Sung, Y.S. Kim, C.R. Park, Facile preparation of reduced graphene oxide-based gas barrier films for organic photovoltaic devices, Energy Environ. Sci. 7 (2014) 3403–3411. doi:10.1039/C4EE02310B.
[22] Q. Luo, Y. Zhang, C. Liu, J. Li, N. Wang, H. Lin, Iodide-reduced graphene oxide with dopant-free spiro-OMeTAD for ambient stable and high-efficiency perovskite solar cells, J. Mater. Chem. A. 3 (2015) 15996–16004. doi:10.1039/C5TA02710A.
[23] A.L. Palma, L. Cinà, S. Pescetelli, A. Agresti, M. Raggio, R. Paolesse, F. Bonaccorso, A. Di Carlo, Reduced graphene oxide as efficient and stable hole transporting material in mesoscopic perovskite solar cells, Nano Energy. 22 (2016) 349–360. doi:10.1016/j.nanoen.2016.02.027.
[24] G. Kakavelakis, T. Maksudov, D. Konios, I. Paradisanos, G. Kioseoglou, E. Stratakis, E. Kymakis, Efficient and Highly Air Stable Planar Inverted Perovskite Solar Cells with Reduced Graphene Oxide Doped PCBM Electron Transporting Layer, Adv. Energy Mater. 7 (2017) 1602120. doi:10.1002/aenm.201602120.
[25] M.G. Helander, M.T. Greiner, Z.B. Wang, Z.H. Lu, Pitfalls in measuring work function using photoelectron spectroscopy, Appl. Surf. Sci. 256 (2010) 2602–2605. doi:10.1016/j.apsusc.2009.11.002.
[26] A. Capasso, F. Matteocci, L. Najafi, M. Prato, J. Buha, L. Cinà, V. Pellegrini, A.D. Carlo, F. Bonaccorso, Few-Layer MoS2 Flakes as Active Buffer Layer for Stable Perovskite Solar Cells, Adv. Energy Mater. 6 (2016) 1600920. doi:10.1002/aenm.201600920.
[27] G.H. Carey, A.L. Abdelhady, Z. Ning, S.M. Thon, O.M. Bakr, E.H. Sargent, Colloidal Quantum Dot Solar Cells, Chem. Rev. 115 (2015) 12732–12763. doi:10.1021/acs.chemrev.5b00063.

[28] P.R. Brown, D. Kim, R.R. Lunt, N. Zhao, M.G. Bawendi, J.C. Grossman, V. Bulović, Energy Level Modification in Lead Sulfide Quantum Dot Thin Films through Ligand Exchange, ACS Nano. 8 (2014) 5863–5872. doi:10.1021/nn500897c.
[29] P.R. Brown, R.R. Lunt, N. Zhao, T.P. Osedach, D.D. Wanger, L.-Y. Chang, M.G. Bawendi, V. Bulović, Improved Current Extraction from ZnO/PbS Quantum Dot Heterojunction Photovoltaics Using a MoO3 Interfacial Layer, Nano Lett. 11 (2011) 2955–2961. doi:10.1021/nl201472u.
[30] A. Stavrinadis, S. Pradhan, P. Papagiorgis, G. Itskos, G. Konstantatos, Suppressing Deep Traps in PbS Colloidal Quantum Dots via Facile Iodide Substitutional Doping for Solar Cells with Efficiency >10%, ACS Energy Lett. 2 (2017) 739–744. doi:10.1021/acsenergylett.7b00091.
[31] J.M. Luther, M. Law, Q. Song, C.L. Perkins, M.C. Beard, A.J. Nozik, Structural, Optical, and Electrical Properties of Self-Assembled Films of PbSe Nanocrystals Treated with 1,2-Ethanedithiol, ACS Nano. 2 (2008) 271–280. doi:10.1021/nn7003348.
[32] C. Powell, X-ray Photoelectron Spectroscopy Database XPS,Version 4.1, NIST Standard Reference Database 20, (1989).
[33] Y. Su, V.G. Kravets, S.L. Wong, J. Waters, A.K. Geim, R.R. Nair, Impermeable barrier films and protective coatings based on reduced graphene oxide, Nat. Commun. 5 (2014) 4843.
[34] Z. Liu, S.P. Lau, F. Yan, Functionalized graphene and other two-dimensional materials for photovoltaic devices: device design and processing, Chem. Soc. Rev. 44 (2015) 5638–5679. doi:10.1039/C4CS00455H.
[35] P. Fontaine, M. Goldmann, F. Rondelez, Influence of Headgroup Cross-Linking on Chain Packing in Langmuir Monolayers of *n* -Alkyltrialkoxysilanes, Langmuir. 15 (1999) 1348–1352. doi:10.1021/la9809933.
[36] S.R. Carino, H. Tostmann, R.S. Underhill, J. Logan, G. Weerasekera, J. Culp, M. Davidson, R.S. Duran, Real-Time Grazing Incidence X-ray Diffraction Studies of Polymerizing *n* -Octadecyltrimethoxysilane Langmuir Monolayers at the Air/Water Interface, J. Am. Chem. Soc. 123 (2001) 767–768. doi:10.1021/ja0057777.
[37] N.A. Manshor, Q. Wali, K.K. Wong, S.K. Muzakir, A. Fakharuddin, L. Schmidt-Mende, R. Jose, Humidity versus photo-stability of metal halide perovskite films in a polymer matrix, Phys. Chem. Chem. Phys. 18 (2016) 21629–21639. doi:10.1039/C6CP03600G.
[38] Y. Yang, J. You, Make perovskite solar cells stable, Nature. 544 (2017) 155–156. doi:10.1038/544155a.
[39] Y. Guo, C. Liu, H. Tanaka, E. Nakamura, Air-Stable and Solution-Processable Perovskite Photodetectors for Solar-Blind UV and Visible Light, J. Phys. Chem. Lett. 6 (2015) 535–539. doi:10.1021/jz502717g.
[40] H. Lu, W. Tian, F. Cao, Y. Ma, B. Gu, L. Li, A Self-Powered and Stable All-Perovskite Photodetector–Solar Cell Nanosystem, Adv. Funct. Mater. 26 (2016) 1296–1302. doi:10.1002/adfm.201504477.
[41] S. Lee, Y.K. Kim, J. Jang, Long-term stability improvement of light-emitting diode using highly transparent graphene oxide paste, Nanoscale. 8 (2016) 17551–17559. doi:10.1039/C6NR05173A.

Supplementary Material

Reduction of moisture sensitivity of PbS quantum dot solar cells by incorporation of reduced graphene oxide

Beatriz Martín-García,[a] Yu Bi,[b] Mirko Prato,[a] Davide Spirito,[a] Roman Krahne,[a] Gerasimos Konstantatos[b,c] and Iwan Moreels [a,†,]*

[a]Istituto Italiano di Tecnologia, Via Morego, 30, 16163 Genova, Italy.

[b]ICFO-Institut de Ciencies Fotoniques. The Barcelona Institute of Science and Technology, Av. Carl Friedrich Gauss 3, 08860 Castelldefels (Barcelona), Spain.

[c]ICREA-Intitucio Catalana de Recerca I Estudis Avancats, Lluis Companys 23, 08010 Barcelona, Spain.

Present Address:

†Iwan Moreels. Department of Chemistry, Ghent University. Krijgslaan 281-S3, 9000 Gent, Belgium.

Corresponding authors:

*Iwan Moreels. E-mail: iwan.moreels@ugent.be

Materials preparation: PbS quantum dots and PbS-rGO.

Materials. PbO (99.999%), oleic acid (OA, 90%), 1-octadecene (ODE, 90%), hexamethyldisilathiane (TMS, synthesis grade), 1-ethyl-3-methylimidazolium iodide (EMII, 97%), 1,2-ethanedithiol (EDT, 98%), ethanol (≥99.8, without additive) and 3-mercaptopropyltrimethoxysilane (MPTS, 95%) were purchased from Sigma-Aldrich. Acetone, toluene, methanol and acetonitrile (ACN) were purchased from Panreac Quimica S.L.U. Au pellets (99.999%) were purchased from Kurt J. Lesker.

Synthesis of colloidal PbS QDs. The synthesis of colloidal PbS QDs with a first absorption peak in the range of 870-930 nm was performed according to established protocols.[1] We mixed PbO (0.45-0.465 g), oleic acid (1.26-2.5 mL) and octadecene (ODE) (10-17.56 mL), and heated and degassed under vacuum at 95 ºC for several hours, obtaining a clear solution. The flask was then heated to 100-120 ºC and a mixture of hexamethyldisilathiane (207 μL) and ODE (10 mL) was rapidly injected. The QD suspension as obtained from synthesis was purified (in air) by adding acetone, followed by centrifugation. The QDs were finally dispersed in toluene and filtered with a 0.2 μm PTFE filter membrane (Sartorius). A QD concentration of 30 $mg.mL^{-1}$ was used for the solar cell fabrication.

PbS-rGO preparation. Reduced graphene oxide (rGO) was obtained from GO by a slight modification of Hummers' method[2,3] using graphite flakes as starting source. The modification consists of increasing the time, from 30min to 15h, to stir the graphite/H_2SO_4/$NaNO_3$/$KMnO_4$ paste in order to improve the exfoliation and oxidation of the graphite. The chemical reduction of GO (0.1 mg mL^{-1} aqueous dispersion at pH=10, adjusted by NH_3 addition) was carried out using caffeic acid (CA), in a weight ratio of 1:1 reductant:GO, at 95ºC during 3h, based on a procedure proposed by Bo *et al.*[4] The rGO was collected as a powder by centrifugation at 9000 rpm during

1h, and subsequently washed with ethanol to remove the CA excess. Finally, the dispersion is centrifuged again at 9000 rpm during 1 hour, after which the rGO powder was dried in an oven at 60ºC overnight.

For the silane functionalization,[3] 0.5 mg.mL^{-1} of rGO were dispersed in ethanol by sonication, and refluxed at 60ºC with 250 µL of MPTS added per mg of rGO during 15h. After synthesis, we precipitated the silane-functionalized rGO by centrifugation (9000 rpm), redispersed it in EtOH by vortexing, and repeated the centrifugation (9000 rpm) to remove unreacted silane. Finally, the silane-functionalized rGO is dispersed in EtOH by sonication (30 min) at a concentration of 0.5 mg.mL^{-1}.

The PbS-rGO materials were prepared, just before solar cell fabrication, by mixing QDs dispersed in toluene with silane-functionalized rGO in EtOH in a ratio of 0.8 nmol QDs per µg rGO. After vigorous stirring during 2 min, the PbS QDs were coupled to the rGO flakes (**Fig. S1a**), and the resulting hybrid material was precipitated by centrifugation and redispersed in EtOH by vortexing, finally yielding a dispersion at a concentration of 50 mg.mL^{-1} (total weight of PbS QDs and rGO).

Electron microscopy characterization of the PbS-rGO materials.

For the preparation of the hybrid material, PbS-rGO, the QD coverage of the rGO flakes was evaluated by transmission electron microscopy (TEM, 100 kV JEOL JEM-1011 microscope, samples were drop casted on carbon-coated copper grids) as previously reported.[3] With a concentration of 0.8 nmol QDs per µg rGO, a complete QD coverage of the flakes is achieved (**Fig. S1a**).

For the scanning electron microscopy (SEM, FEI Helios Nanolab 600 DualBeam microscope) characterization of the PbS-rGO films (**Fig. S1b**), we performed the measurements directly on solar cell devices (areas outside the Au top contacts). From the SEM image, we observed a good coverage of the PbS-rGO film. Zooming into the PbS-rGO sheets (**Fig. S1c**), and comparing with pure rGO sheets (**Fig. S1d**), the additional roughness observed in the SEM images indicates the presence of PbS QDs on the rGO sheets, as a uniform layer and without large PbS QD agglomerates after EDT ligand exchange. The thickness of the PbS_{EMII} / PbS_{EDT} / $PbS\text{-}rGO_{EDT}$ stack was evaluated by SEM measurements of the solar cell cross section (sample prepared by focused ion beam). The PbS-rGO solar cell has a total PbS absorber layer thickness of 254 nm (**Fig. S1e**). A PbS reference device yielded 220 nm for the PbS absorber layer (**Fig. S1f**), consistent with 200 nm of PbS_{EMII} and 20 nm of PbS_{EDT}[1]. From these measurements, considering also that we only spin-coated 1 layer of PbS_{EDT} in the PbS-rGO solar cells (i.e. 10 nm), we inferred a PbS-rGO layer thickness of 44 nm.

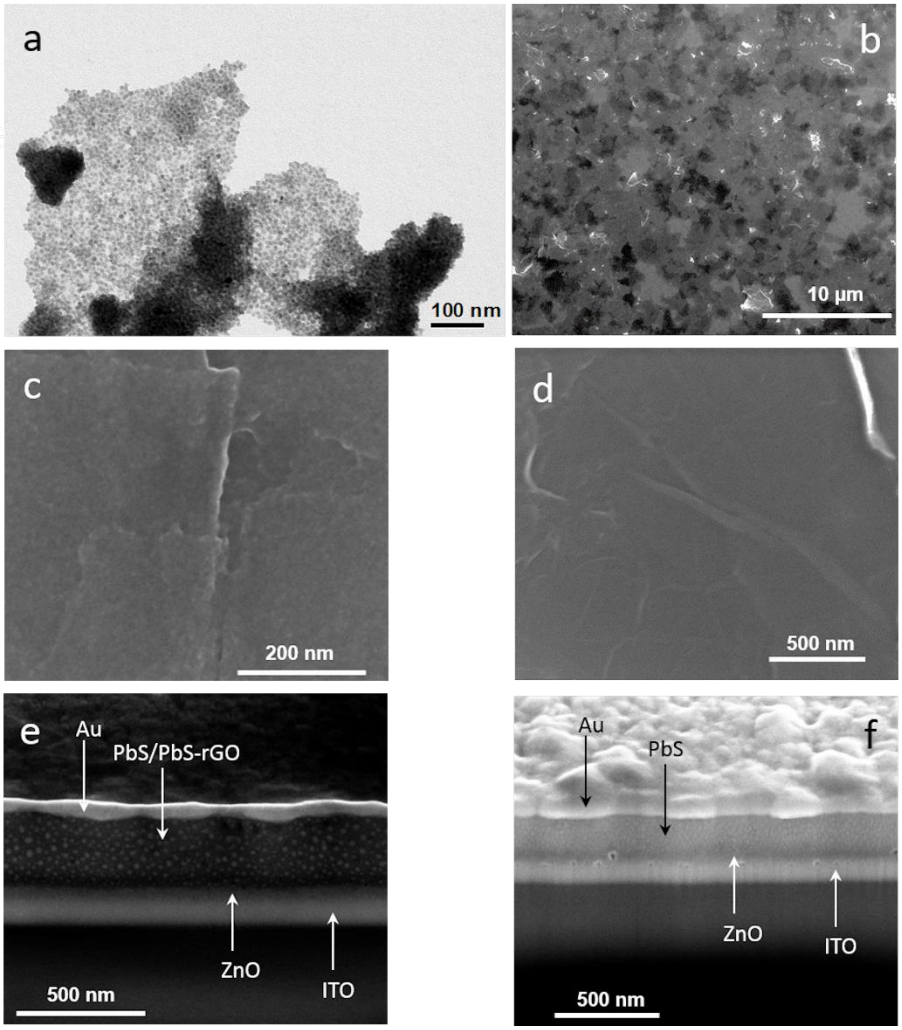

Fig. S1. *(a) Representative TEM image of the PbS-rGO hybrid. (b) Representative SEM image of a PbS-rGO$_{EDT}$ film deposited as part of the PbS-rGO solar cell (imaged area lies outside Au top contact). (c) SEM image of the top view of a PbS-rGO solar cell (area outside of Au top contact) showing the increased roughness when PbS QDs are attached to the rGO sheets. (d) SEM image of pure rGO sheets deposited by dropcasting on silicon substrates. (e) Cross section of the optimized PbS-rGO solar cell, consisting of Au contact/PbS-rGO$_{EDT}$ (1 layer)/ PbS$_{EDT}$ (1 layer)/PbS$_{EMII}$ (12 layers)/ZnO/ITO/glass. (f) Cross section of the PbS reference cell, consisting of Au contact/PbS$_{EDT}$ (2 layers)/PbS$_{EMII}$ (12 layers)/ZnO/ITO/glass.*

***I-V* measurements on PbS-rGO films.**

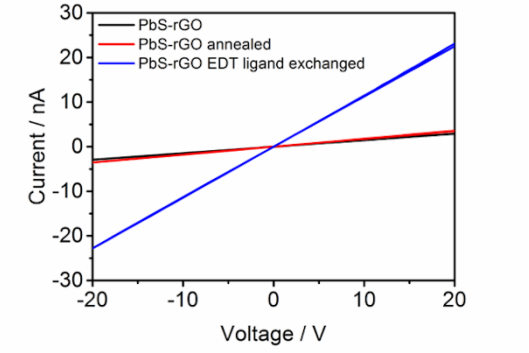

Fig. S2. *Current vs. voltage of a PbS-rGO hybrid film (120 nm thickness) before (black line) and after annealing (80°C) (red line), and after EDT ligand exchange (blue line).*

To evaluate how we can enhance the conductivity of the PbS-rGO hybrid material, we measured the current as a function of applied voltage on PbS-rGO films (120 nm thickness) deposited on glass by spin coating. The films were contacted by two drops of silver paste, separated at a distance of about 7 mm. The initial PbS-rGO film yielded a conductance G of 0.15 nS, which increased after annealing at 80 °C to 0.17 nS. A more significant increase to G = 1.10 nS was observed after EDT ligand exchange (factor of 7.6).

UPS measurements on ligand-exchanged PbS QDs and PbS-rGO hybrid material.

The ultraviolet photoelectron spectra (UPS) were acquired on spin-coated EMII-treated PbS QD, EDT-treated PbS QD and PbS-rGO$_{EDT}$ films, deposited on Au-coated silicon substrates (**Fig. S3)**. The UPS yielded a valence band maximum (VBM) energy of -5.4, -5.1 and -5.1 eV vs. vacuum level, respectively. By adding the band gap value of 1.3 eV, we obtained a conduction band minimum (CBM) energy of -4.1, -3.8 and -3.8 eV, respectively.

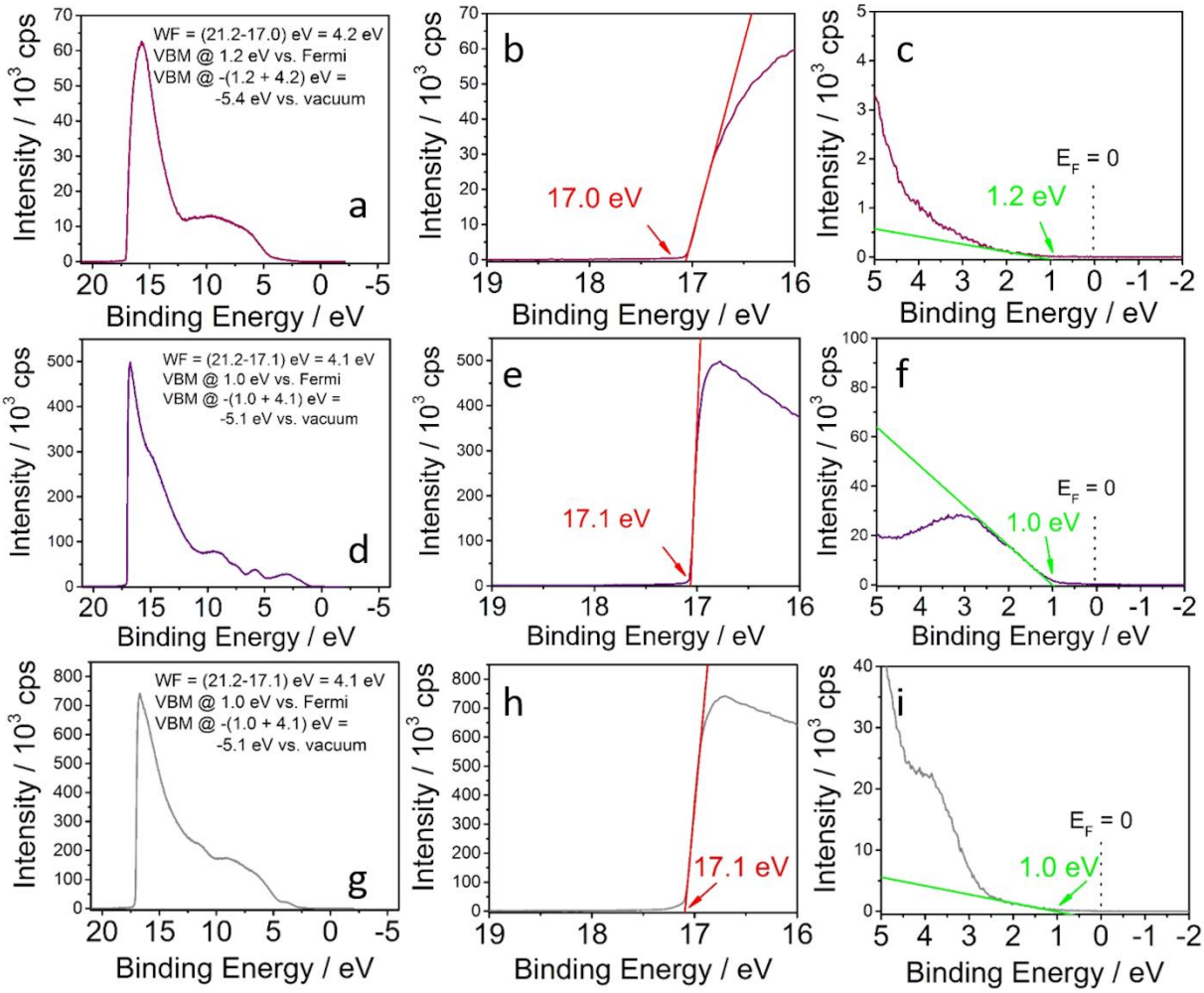

Fig. S3. *UPS acquired on EMII-treated PbS QD (a-c), EDT-treated PbS QD (d-f) and PbS-rGO$_{EDT}$ (g-i) films, spin coated on 50 nm Au-coated silicon substrates. A WF of -4.2, -4.1 and -4.1 eV, respectively, was determined from the threshold energy (fit shown in red) of the emission of secondary electrons upon He I excitation (21.2 eV). A VBM of -5.4, -5.1 and -5.1 eV vs. vacuum level was calculated from the low binding energy onset of the UP spectrum, corresponding to the VB maximum distance from the Fermi level (fit shown in green), which was then subtracted from the WF.*

Solar cell stack optimization.

In **Table S1** we include the relevant parameters of the solar cells with PbS-rGO$_{EDT}$ integrated in different positions (see also main text, **Fig. 1b**).

Parameter tested	V_{OC} / V	J_{sc} / mA cm^{-2}	FF	PCE / %	R_{shunt} /kΩ	R_{series} / Ω
Reference 12 layers QD$_{EMII}$ / 2 layers QD$_{EDT}$	0.55 ± 0.03	20.7 ± 1.0	0.57 ± 0.03	6.52 ± 0.33	9.8 ± 0.5	63 ± 3
1 layer PbS-rGO	0.42 ± 0.02	11.7 ± 0.6	0.38 ± 0.02	1.90 ± 0.10	3.1 ± 0.2	183 ± 9
2 layers PbS-rGO	0.37 ± 0.02	11.0 ± 0.6	0.50 ± 0.03	2.03 ± 0.10	6.3 ± 0.3	61 ± 3
1 layer QD$_{EDT}$ / 1 layer PbS-rGO	0.52 ± 0.03	16.4 ± 0.8	0.54 ± 0.03	4.56 ± 0.23	7.8 ± 0.4	55 ± 3

Table S1. *Performance of the different solar cells that include the PbS-rGO hybrid material. All cells contain 12 layers of QD$_{EMII}$. The 2 layers of QD$_{EDT}$ were replaced by 1 layer of PbS-rGO, 2 layers or PbS-rGO and 1 layer QD$_{EDT}$ / 1 layer PbS-rGO respectively.*

Solar cell shelf life.

To test the shelf life, the solar cells were stored in the dark under ambient atmosphere (R.H. 40-60%).

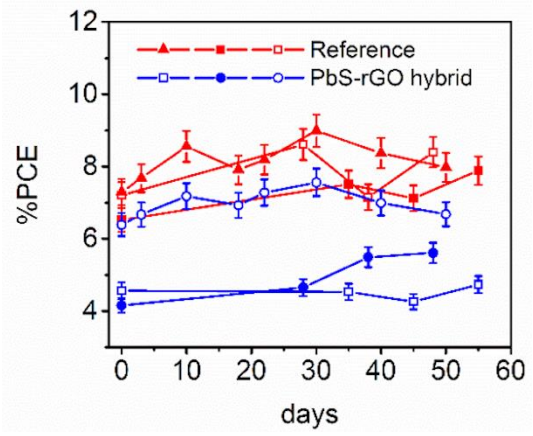

Fig. S4. *Evolution the solar cell PCE under storage in the dark. Both the three reference solar cells (red) and three PbS-rGO solar cells (blue) show a similar rise of the PCE.*

Continuous illumination and water-saturated environment tests.

Complementary photovoltaic characteristics (J_{sc}, V_{oc} and FF) for the solar cells, measured for continuous light exposure and exposure to humid atmosphere (R.H. 100%) are shown in **Fig. S5** and **Fig. S6**, respectively.

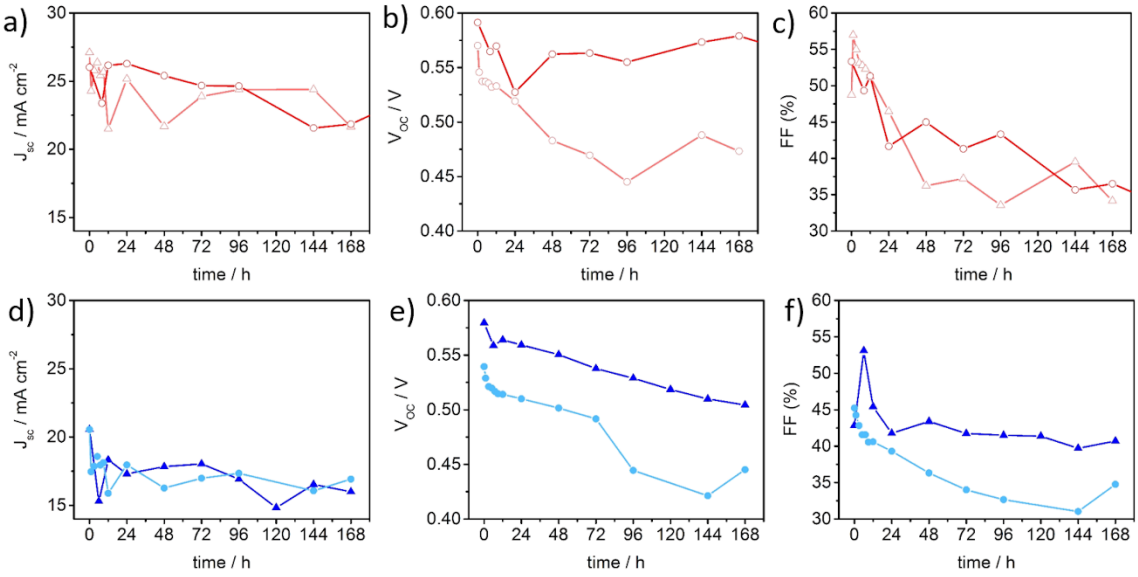

Fig. S5. *Evolution of 4 different PV cells in terms of J_{sc} (a, d), V_{oc} (b, e) and FF (c, f) for the PbS reference cells (red, a-c) and the PbS-rGO solar cells (blue, d-f), under continuous illumination (1 sun) at ambient conditions. Data are an average from 3 different contacts in each sample (in total 12 devices were evaluated).*

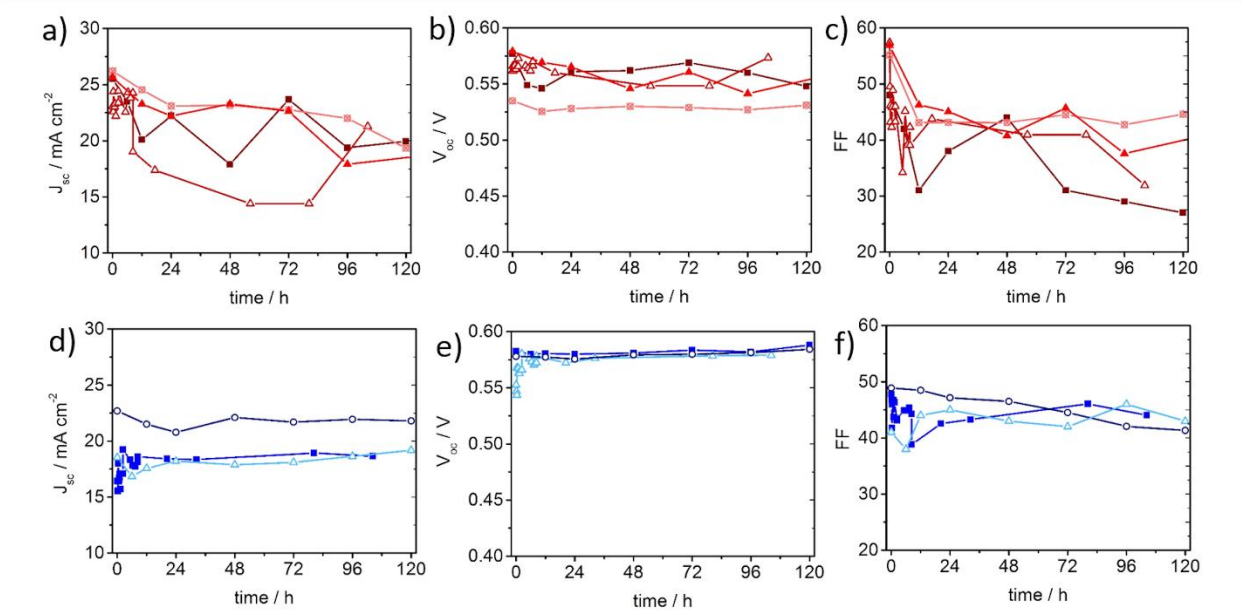

Fig. S6. *Evolution of 7 different PV cells in terms of J_{sc} (a, d), V_{oc} (b, e) and FF (c, f) for PbS reference cells (red, a-c) and PbS-rGO solar cells (blue, d-f), when stored under saturated water vapor atmosphere. Data are an average from 3 different contacts in each sample (in total 21 devices were evaluated).*

Influence of moisture on the PbS absorber layer: supplementary SEM/EDX analysis.

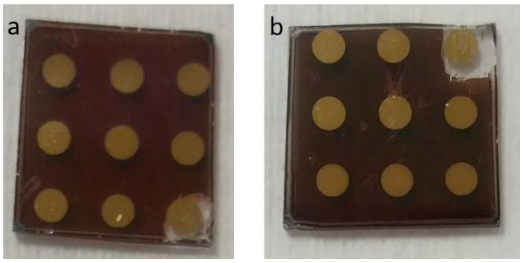

Fig. S7. *Representative pictures of PbS reference cells (a) and PbS-rGO cells (b) before moisture exposure.*

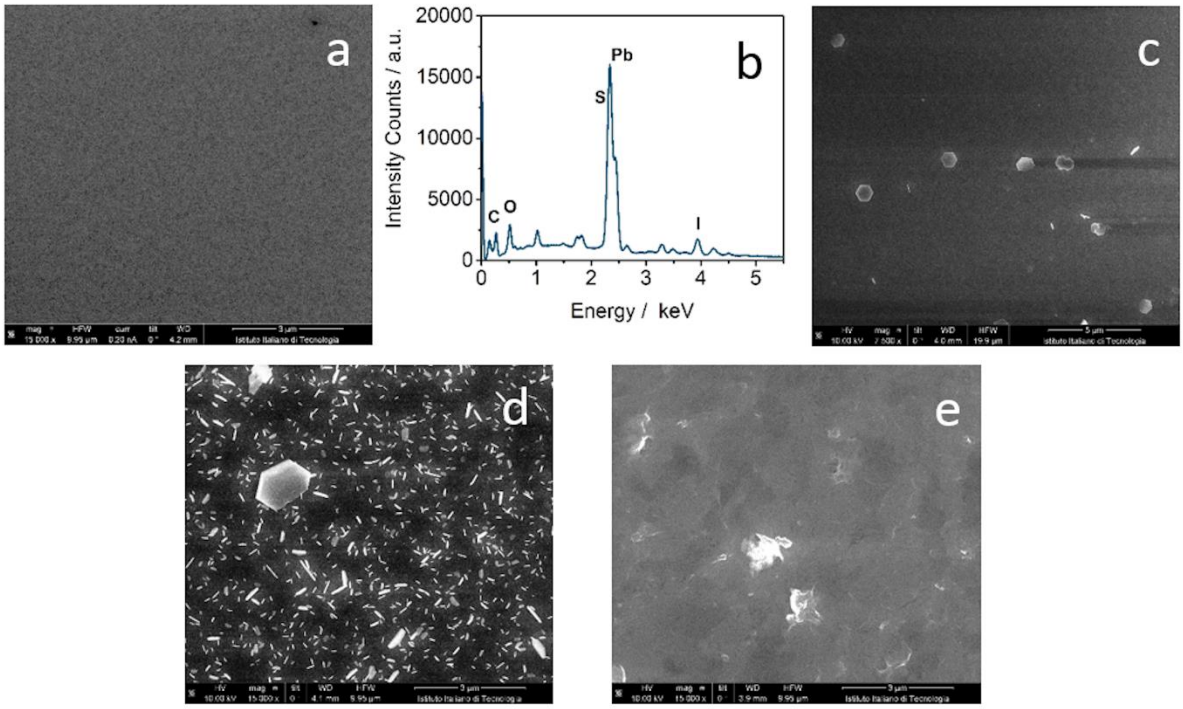

Fig. S8. *(a) Representative SEM image of a PbS reference cell before moisture exposure. (b) The corresponding EDX spectrum, collected over an area of ca. 160x160 µm^2. (c) Representative SEM image of a PbS reference cell after moisture exposure, showing the formation of hexagonal crystals. (d) Representative SEM image after moisture exposure of the PbS_{EMII} / PbS_{EDT} film (reference sample). (e) Representative SEM image after moisture exposure of the PbS_{EMII} / PbS_{EDT} / PbS-rGO_{EDT} film (PbS-rGO sample). Both films were also characterized by XPS (see main text).*

To evaluate the degradation induced by the exposure to moisture, which can be observed in the images in **Fig. 4a-b** in the main text as a white area in the reference cells (initial state is shown in **Fig. S7**), we performed SEM/EDX measurements on the different solar cells. In **Fig. S8a-b**, we include SEM images and EDX spectrum of the reference sample before moisture exposure. See main text for the data after exposure, and the data of the PbS-rGO solar cells. In addition, a SEM image of the hexagonal $PbSO_x$ crystals is included in **Fig. S8c**. To monitor the surface oxidation, we also carried out XPS analysis, performed on spin-coated thin films on glass (see main text). SEM measurements of these films are shown in **Fig. S8d-e**. As for the solar cells, the formation of the hexagonal $PbSO_x$ crystals is again observed only in the reference sample (**Fig. S8d**).

Influence of moisture on the PbS absorber layer: absorbance spectroscopy.

To complement the XPS and SEM/EDX results, we used absorbance spectroscopy (**Fig. S9),** which allows us to evaluate the optical properties of the entire film (in contrast with a surface-sensitive technique such as XPS). We used the same samples already measured for the XPS analysis. Two different films were evaluated: one consisting of PbS QDs only (reference sample, PbS_{EMII} (12L) /PbS_{EDT} (2L)), and one where we integrated the PbS-rGO hybrid material as the final layer (PbS-rGO integrated, PbS_{EMII} (12L) / PbS_{EDT} (1L) / PbS-rGO_{EDT} (1L)). The films were deposited directly on glass substrates.

Two samples from each group were used for moisture exposure (5 days), meanwhile for each kind of film we kept a sample stored in a N_2-filled globe box. In **Fig. S9c-d**, we observed a blue shift on the first excitonic peak of the PbS QDs, from ca. 971 nm to 947 nm, after exposure in the case of the reference samples, which can be ascribed to the oxidation of the film.[5] In contrast, the position of the first absorption peak remained constant for the samples that contained the PbS-rGO top layer, supporting again that only the top surface of the PbS-rGO is affected by oxidation (as was observed with XPS) while the bulk is unaffected.

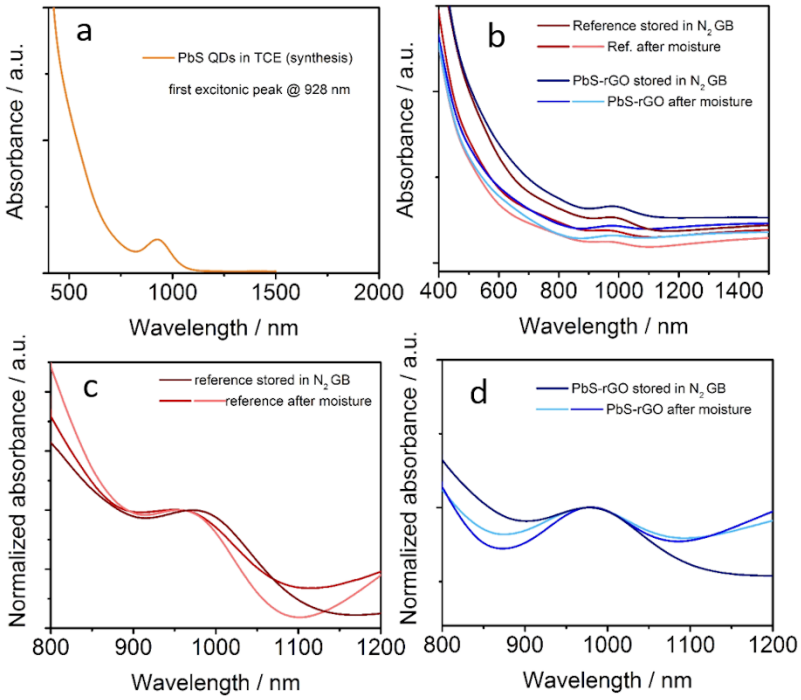

Fig. S9. *(a) Absorbance spectrum of the PbS QDs, dispersed in tetrachloroethylene, which were used to prepare the films. (b) Absorbance spectra of the different reference (red) and PbS-rGO (blue) films measured: without moisture exposure (samples stored in N_2 globe box) and after 5*

days of water-saturated vapor exposure. (c, d) Corresponding normalized absorbance spectra of the PbS (c) and PbS-rGO (d) films. Only in panel (c), a blue shift is observed.

References

[1] Y. Cao, A. Stavrinadis, T. Lasanta, D. So, G. Konstantatos, The role of surface passivation for efficient and photostable PbS quantum dot solar cells, Nat. Energy. 1 (2016) 16035.

[2] W.S. Hummers, R.E. Offeman, Preparation of Graphitic Oxide, J. Am. Chem. Soc. 80 (1958) 1339.

[3] B. Martin-Garcia, A. Polovitsyn, M. Prato, I. Moreels, Efficient charge transfer in solution-processed PbS quantum dot-reduced graphene oxide hybrid materials, J. Mater. Chem. C. 3 (2015) 7088–7095. doi:10.1039/C5TC01137J.

[4] Z. Bo, X. Shuai, S. Mao, H. Yang, J. Qian, J. Chen, J. Yan, K. Cen, Green preparation of reduced graphene oxide for sensing and energy storage applications, Sci. Rep. 4 (2014) 4684.

[5] C.-H.M. Chuang, P.R. Brown, V. Bulović, M.G. Bawendi, Improved performance and stability in quantum dot solar cells through band alignment engineering, Nat. Mater. 13 (2014) 796–801. doi:10.1038/nmat3984.